

Air Entrapment and its effect on Pressure Impulses in the slamming of a Flat Disc on Water

Utkarsh Jain^{1†}, Patricia Vega-Martínez² and Devaraj van der Meer¹

¹Physics of Fluids Group and Max Planck Center Twente for Complex Fluid Dynamics, MESA+ Institute and J. M. Burgers Centre for Fluid Dynamics, University of Twente, P.O. Box 217, 7500AE Enschede, The Netherlands

²Fluid Mechanics Group, Universidad Carlos III de Madrid, Leganés, Spain

(Received xx; revised xx; accepted xx)

The presence of ambient air in liquid-slamming events plays a crucial role in influencing the shape of the liquid surface prior to the impact, and the distribution of loads created upon impact. We study the role of trapped air in a simplified geometry by slamming a flat disc on a stationary water bath. We show how air trapping influences pressure peaks at different radial locations on the disc, how the pressure impulses are affected, and whether local pressure impulses differ from area-integrated (force) impulses due to impact. We emphasize that pressure impulses are a much more faithful indicator of the intensity of an impact event, being less affected by transients in the signals, and obeying the relevant inertial length and time scales.

Key words:

1. Introduction

Situations involving the impact of a liquid on solid, or vice-versa are commonly found in several industrial applications. Some notable examples that occur on a large scale are hull slamming during the (re-)entry of a ship into water (Kapsenberg 2011), the landing of sea-planes or spacecraft (Abrate 2013), wet-deck slamming in ships or off-shore structures (Smith *et al.* 1998; Faltinsen 2000; Faltinsen *et al.* 2004), and wave impacts on harbours and sea-walls (Peregrine 2003), and during sloshing (Dias & Ghidaglia 2018). Liquid-solid impact events are associated with large loads that are created primarily due to the added mass effect: upon impact, a certain mass of liquid is rapidly accelerated towards the velocity of the impacting object. However in all situations, the surrounding air can have a very non-trivial influence on the generated load, and its distribution on the solid structure (Dias & Ghidaglia 2018; Bogaert *et al.* 2010). One way this occurs is via aeration of the liquid phase (Bredmose *et al.* 2015; Ma *et al.* 2016). More often, the air that is trapped in between the liquid and the solid affects the shape of the liquid surface (Hicks *et al.* 2012), and also plays a crucial role in affecting the loading on the solid phase (Bredmose *et al.* 2009; Peregrine & Thais 1996; Wood *et al.* 2000; Hattori *et al.* 1994; Ermanyuk & Ohkusu 2005). We focus on the latter in the present work. Its role in influencing the pressures can be benign, such as by mitigating pressure singularities and

† Email address for correspondence: u.jain@utwente.nl

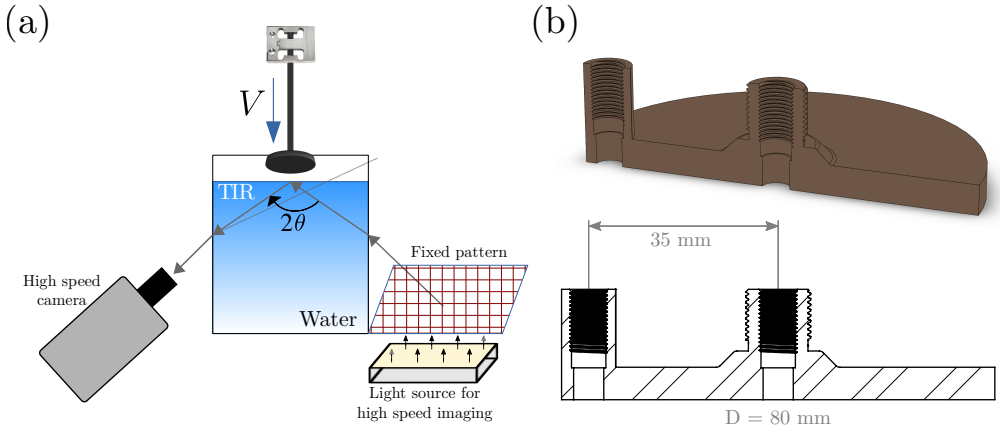


FIGURE 1. (a) Schematic of the setup. A linear motor is used to impact a disc on water surface with constant velocity. Using total internal reflection (TIR), the water surface can be used as a mirror, and its behaviour observed when subjected to deflections. A load cell is installed along the rod to measure the overall force experienced in the vertical direction. (b) Design and dimensions of an 80 mm wide disc on whose surface local impact pressures are measured.

distributing the loads over a larger surface. On the contrary, the trapped air may also increase the load by oscillations or even produce significant damage on a solid structure by cavitation implosion.

Here we experimentally study the local pressures and forces produced on a disc that is impacted onto a water bath. Prior to the impact, the disc creates an air flow that results in it entrapping air on the impacting side of its own accord (Verhagen 1967; Jain 2020). We describe the setup and the air trapping on the disc in section 2. The trapped air layer has been shown to cause a small reduction in the peak pressure (Chuang 1966) and also affect its distribution (Okada & Sumi 2000; Tödter *et al.* 2020) over the impacting face. In section 3, we report the measurements of local pressures at the centre of the disc and near its edge (see figure 1), and how the trapped air influences peak pressures. The discussion in this section is further complemented in section 4 by measuring the total impact force on the assembly with a load cell. The peak values of both are found to be very sensitive to the temporal resolution of the equipment. We compute impulses from these measurements, and find their behaviour to be much more repeatable than mere peak values of pressures and forces. The early growth of impact impulses is shown to be inertial, suggesting that added mass effect plays a dominant role during this stage. Impact force impulses measured using the two approaches are compared with results from analytical and numerical models.

2. Setup

The experimental installation consists of a reservoir filled with water, which is contained in a tank of area $50 \text{ cm} \times 50 \text{ cm}$. The water depth is kept fixed at 30 cm. We impact flat discs on the water bath such that their impacting surface is parallel to the stationary water surface. The disc's motion across the free surface is controlled using a linear motor, with a position accuracy of approximately $0.6 \mu\text{m}$. The assembly's motion is programmed such that it achieves a specified velocity when in the middle of its available stroke. Concerning the disc, the stroke is programmed such that it attains the constant, programmed-for velocity V , several diameters before it reaches the free surface. This

constant velocity is maintained as the disc plunges roughly the same distance into the target pool. V is varied from 0.05 – 3 m/s.

The free surface of water is visualised using the total internal reflection (TIR) setup as shown by the schematic in figure 1a (Jain *et al.* 2020a,b). When the disc and water surface are in touch, those sections of the free surface that wet the disc cease to reflect the reference pattern and effectively disappear.

We install pressure sensors on an 80 mm wide disc made of steel to measure pressures on its impacting surface. Vaseline is used to seal any gaps between the sensors and the mounting sites on the disc. The sensors used were Kistler 601CAA dynamic piezoelectric transducers, with a diaphragm width of 5.5 mm. They were flush mounted on the disc as per the manufacturer’s instructions. A sketch showing the dimensions of the disc and positions of the sensors is shown in figure 1(b). Pressure measurements were made at an acquisition frequency of 200 kHz. Additionally we also measure the overall force on the disc that is generated at impact using a strain gauge load cell (FUTEK LSM300). It is calibrated using known weights, and the measurements are done at an acquisition rate of 25 kHz. Disc radii R are varied from 1–8 cm.

3. Spatially localised loading

As the disc approaches the water surface with a finite speed, there is an intervening air layer trapped between the two. The air in this layer is squeezed out such that its flow results in a radial pressure gradient. These pressure changes are sufficiently large to deform the water surface before the disc makes any contact with it. Thus the water surface is made aware of the approaching disc in advance; at the point that lies directly under the disc centre, the liquid surface is pushed down by stagnation pressure. Conversely under the disc edge, a high hydrodynamic pressure creates a suction which destabilises the water surface to be sucked upwards towards the disc (Jain 2020). As a result at the first moment of the disc making contact with the water surface the water-air surface under the disc edge is vertically separated from that under the disc centre by approximately 200 μm . This ‘air-cushioning’ effect on the free surface invariably creates conditions to trap an air layer under the disc at its first contact with the liquid surface, as is shown in figures 2 and 3.

At low V , such as shown in figure 2 at 0.06 m/s and 0.1 m/s, the air layer merely contracts inwards on account of high surface tension of the air-water interface. Notice that as the surrounding water displaces air, its perimeter stays remarkably stable and consistent in shape. This is due to the interface being stabilised by Saffman-Taylor mechanism, which is only unstable to perturbations when a less viscous liquid displaces a more viscous one. Notice how at a slightly higher V of 0.1 m/s in figure 2(b) the air film is briefly ruptured as it passes over the sensor at the disc edge, but then continues to contract inwards preserving the interface shape to remain as a bubble at the disc centre. Our observations of how such a trapped air bubble behaves are consistent with the observations of Mayer & Krechetnikov (2018), who used a flat rectangular plate as the impactor.

At higher impact velocities (figure 3), after the air film is trapped at the first moment of impact, it initially starts to collapse towards the disc centre. However, it is quickly penetrated by the liquid near the disc centre due to a high stagnation pressure in the liquid (see Movies 3 and 4 for the process at $V = 1.0$ m/s).

The differences in pressure characteristics in a constant presence of the air film, and when its expelled from under the disc, are discussed next.

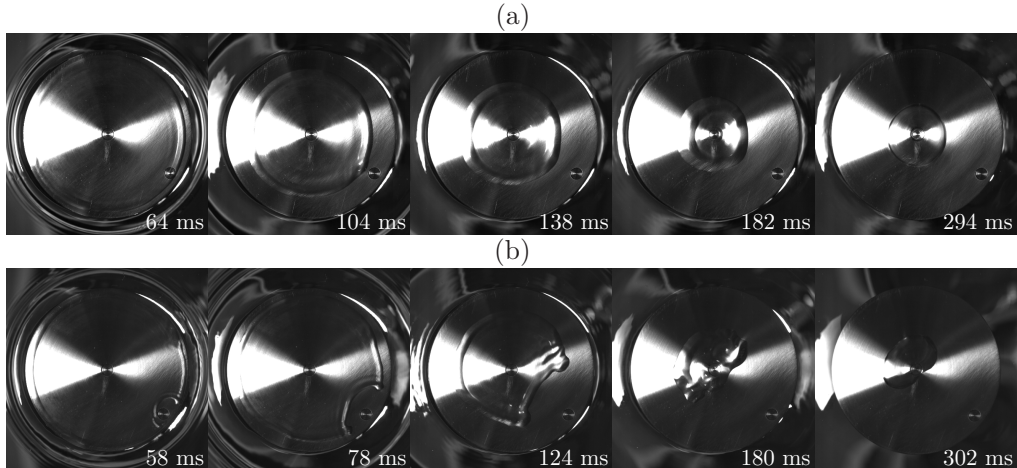


FIGURE 2. The trapping of an air film on a water-entering disc is directly seen from below the water bath at $V = 0.06$ m/s in panels (a), and at 0.1 m/s in panels (b). The disc shown is 8 cm wide (as shown in figure 1(b)). The time labels are centred at 0 ms when the disc makes its first contact with water. The trapped air film contracts inwards due to surface tension of water air interface. The process is also shown in Movies 1 and 2.

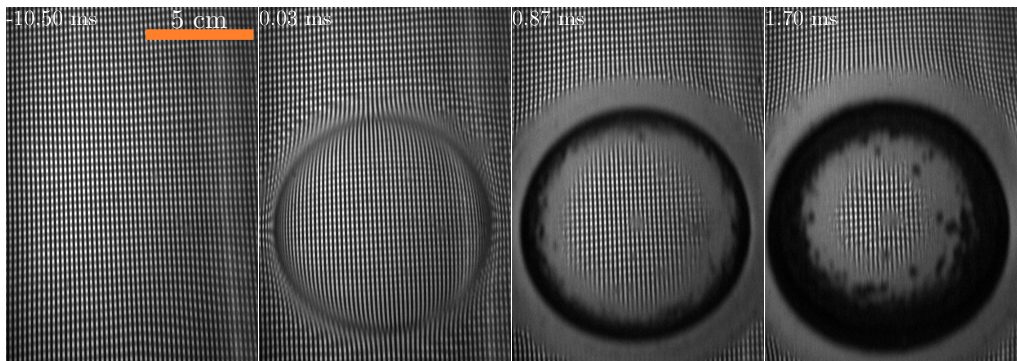


FIGURE 3. Snapshots of the free surface during the impact of a 10 cm wide disc at 1 m/s, as seen using the TIR setup, as shown in figure 1(a), imaging the free surface from below. The moment when the disc makes first contact with the water surface can be identified when a section of the reflecting water surface disappears by wetting the disc. The time labels shown at top left corner are centred about $t = 0$ at the instant where the disc makes first contact with the deformed water surface. An air layer is trapped on the disc at impact. It collapses inwards as the disc plunges further into the liquid bath. Also see Movie 4.

3.1. Pressure measurements

The effect of impact on pressure characteristics are found to be typical of solid-liquid impact events in general (Peregrine 2003; Kapsenberg 2011). The first contact between a transducer on the disc and water surface creates a large pressure spike (figure 4(a,b)), lasting for a short duration $\sim \mathcal{O}(10^{-4})$ s). Note from figure 4(a,b) how in examples shown for both a low velocity impact at $V = 0.075$ m/s, and a larger velocity at 1 m/s, the pressure at disc centre starts to grow prior to that at the edge. This is due to a large stagnation pressure building up in the liquid at the disc centre, whose magnitude is of the order $\rho_w V^2$. A component in the pressure signals with a period of 4 ms is visible

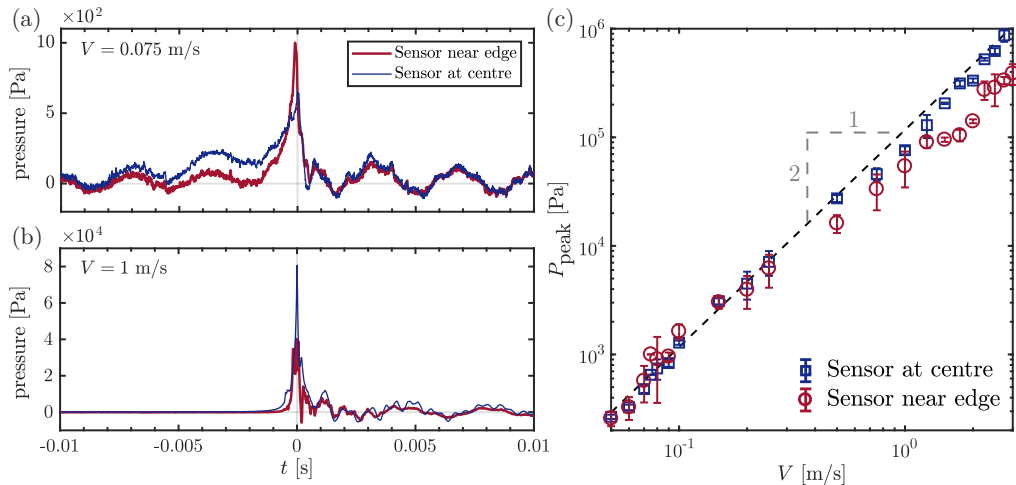


FIGURE 4. Time series of pressures measured at the two locations on an 80 mm wide disc (see figure 1b) when it impacts a deep liquid bath at a velocity of (a) 0.075 m/s and (b) 1.0 m/s. The signals are centred about $t = 0$ at the instant when the central pressure reaches its peak. (c) Peak pressures measured at two locations on the same disc are plotted over a range of impact velocities. Error bars show the standard deviation of peak pressures over 3–6 repetitions of the experiment at each impact velocity. The peak pressures at the centre are found to scale quadratically with V , whereas those near the edge of the disc are found to be slightly below those at the centre. See main text for discussion.

at all times in panel (a), and after the impact in panel (b) in figure 4. This arises from structural oscillations in the disc-rod assembly, and is also present in the data from the load cell (figure 7).

Peak pressures measured from impacts done at a range of velocities are plotted in figure 4(c). Multiple repetitions of the experiment at each velocity were performed to quantify reproducibility. At low velocities ($V \lesssim 0.5$ m/s), pressures at the edge of the disc were found to be higher than those at the disc’s centre. The opposite however was observed in impacts at higher velocities ($V \gtrsim 0.5$ m/s).

Note that peak impact pressures at the disc centre are approximately 100 times larger than the stagnation pressure $\rho_w V^2$ in water (see figure 4(c)). At larger V , the initially trapped air is expelled from under the disc’s edges by the radially outwards flowing liquid (see Movies 3 and 4). Thus, while at *low* velocities the impact pressures at the disc’s centre are actively ‘cushioned’ by the trapped air film, for $V \gtrsim 0.5$ m/s, the air film appears to play a diminished role, if any, in reducing the peak pressure at the disc centre. Okada & Sumi (2000) performed impact tests using a flat plate, and also found higher peak pressures closer to its centre. We thus designate impact velocities $\gtrsim 0.5$ m/s as ‘slamming’ velocities throughout the present work. At slamming velocities, as the air film is violently expelled out from under the disc, the liquid interface breaks up. This introduces greater variation in peak pressures at the disc’s edge, which can be seen from the error bars in figure 4(c).

3.2. Localised pressure-impulses during impact

The most elementary measure of the intensity of an impact event is the peak pressure that is measured on the solid structure. However, in most circumstances, this peak pressure can have a large variance between tests performed at the same parameters. Since rise times of the initial impact peak can be very short $\sim \mathcal{O}(10^{-5}$ s), one reason

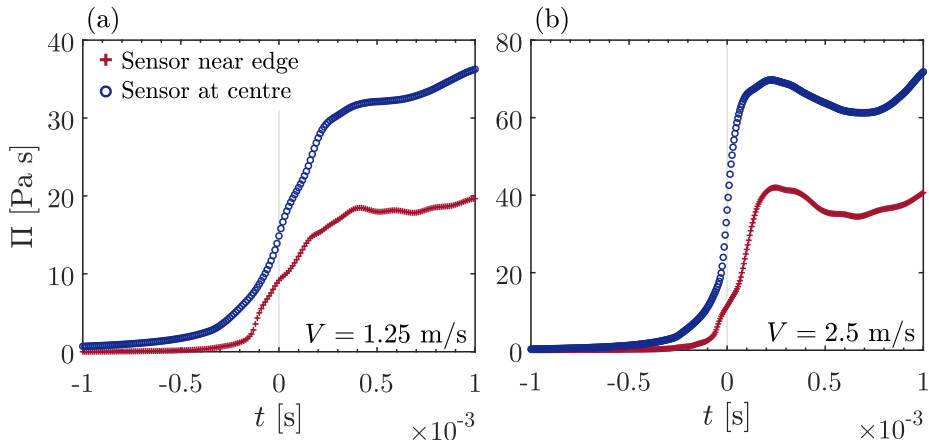


FIGURE 5. Pressure impulses Π measured from experiments at (a) $V = 1.25$ m/s and (b) $V = 2.5$ m/s are plotted as time series. Experiments were done with the sensor arrangement as shown in figure 1b. As before, all time series are centred about $t = 0$ at moment when the pressure at disc centre reaches its maximum.

for the variance in peak pressures is often due to limited time resolution of the sensors. Another reason very often encountered is the inconsistent role played by the ambient air that is trapped at impact. Since the first such work by [Bagnold \(1939\)](#) on studying the effect of trapped air on peak pressures, several later works ([Denny 1951](#); [Chan *et al.* 1988](#); [Peregrine 2003](#)) have also identified that the trapped air can play an important role during the production of the initial large pressure peak. [Richert \(1969\)](#), [Partensky \(1989\)](#) and [Hattori *et al.* \(1994\)](#) found from wave impacts on walls, that the most severe pressures were produced when there were several small air bubbles, or a very thin ‘lens shaped’ air pocket trapped along the wall. It is a general consensus that pressure impulse, or the pressure integrated over duration of the peak, is a better predictor of the amount of local damage that is caused by an impact event on the solid structure ([Bullock *et al.* 2007](#); [Bredmose *et al.* 2009](#); [Hull & Müller 2002](#); [Kirkgöz 1990](#); [Dias & Ghidaglia 2018](#); [Peregrine 2003](#)). Indeed, pressure impulse is also found to be a much more reproducible measure of the intensity of impact than the peak value in itself ([Bagnold 1939](#); [Dias & Ghidaglia 2018](#); [Denny 1951](#); [Chan *et al.* 1988](#); [Peregrine 2003](#); [Bullock *et al.* 2007](#)).

Thus we calculate the pressure impulses $\Pi(t)$ from the measurements done at slamming velocities. They are computed by numerically integrating the pressure signal from a time before it starts to rise t_0 , to arbitrarily later times as

$$\Pi(t) = \int_{t_0}^t p(t') dt'. \quad (3.1)$$

Consistent with all the pressure measurements, the time-coordinate of all pressure-impulse results are again centred about $t = 0$, at the instant when the central pressure reaches its maximum. This way of presenting the results allows one to focus on the early-time rise in impulse until the trapped air film collapses at the disc’s centre.

Pressure impulses measured at $V = 1.25$ and 2.5 m/s are plotted in figure 5. At the disc centre, $\Pi(t)$ starts to rise earlier than at the disc’s edge. This can be ascribed to an observation made earlier in figure 4(a), where it was seen that the pressure at the disc centre starts to rise before than that at the edge. The difference in how impulse at the edge grows compared to that at the centre occurs due to different behaviour of air flow in the two regions at impact. At the moment of impact, there is a trapped air film whose

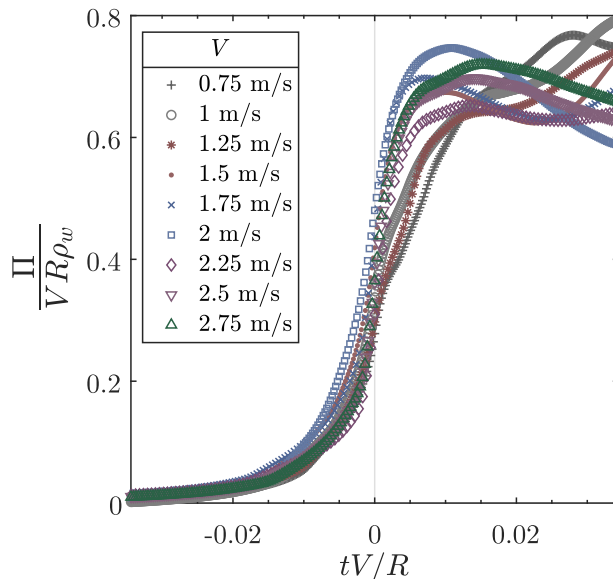


FIGURE 6. Non-dimensional pressure impulses $\hat{\Pi} = \Pi/VR\rho_w$ measured at disc centre (from figure 5) are plotted against non-dimensional time tV/R . The convincing data collapse reveals that the accumulation of pressure impulse at disc centre, when it impacts at high velocities, can be described as an inertial process.

thickness is maximum under the disc centre. The opposite holds true at the disc edge, where the contact first happens. At slamming velocities, after the peak impact pressure is attained, the air film collapses. Immediately after this, the air that was initially trapped is fragmented and expelled from under the disc. As its escape happens from under the disc edge, fast air flow, followed by fast liquid flow, interfere with the pressure reading. That the impulse shown in figure 5 initially accumulates more smoothly at the centre than at the disc's edge suggests that impact at the disc centre is cushioned by the air layer. Indeed, the presence of air also prolongs the duration of the initial impact peak, which contributes to the impulse at the centre growing to larger values than that at disc edge (Iafrafi & Korobkin 2008).

The air film plays this role of a cushioning layer only in the earliest stages of impact before the peak pressure at disc centre reaches its maximum. Thus, whatever subsidiary effect that is caused by it, such as mitigating pressure singularities, distributing the loading, and prolonging the impact, lasts for a short duration of a few milliseconds prior to $t = 0$ in figure 5. This stage is key to determining the final value of impulse that is accumulated during the first impact peak. Noting that inertially, pressure should scale as $\rho_w V^2$, and time as R/V , we expect the pressure impulse $\Pi(t)$ to scale as the product of the former. Using this inertial scaling, we non-dimensionalise the results in figure 5(a) and re-plot them in figure 6. The growth of pressure impulse at the centre is very well collapsed by the non-dimensionalisation. This leads to the surprising conclusion that early-time loading on the pressure sensor grows as it would have, had the pressure sensor already been in touch with, or immersed in the liquid.

This allows us to conclude that at the disc centre, the impact impulse arises mainly due to sudden acceleration of a certain bulk of liquid by the impact. It leads us to expect that the impulse created by total force on the discs' entire surface should behave similarly to the pressure impulses as in figure 6.

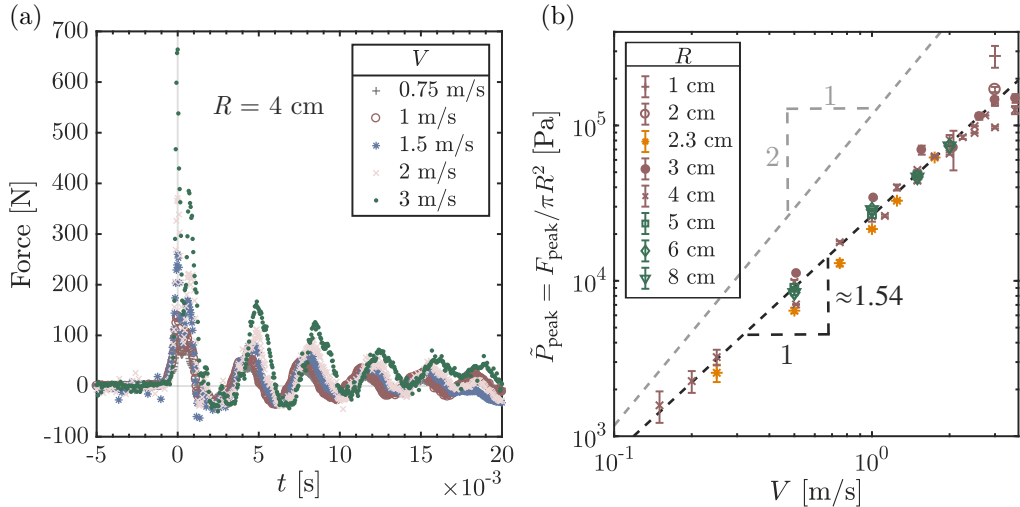


FIGURE 7. (a) Time evolution of the impact force measured using the disc shown in figure 1(b), impacted at various velocities. The time series are centred about $t = 0$ at the time of registering peak impact force. (b) Peak average pressure, $\bar{P}_{\text{peak}} = F_{\text{peak}}/\pi R^2$ computed from the force measured in experiments using discs of varying sizes, materials and impact speeds are plotted against their velocities of impact. Data shown using purple coloured markers are from experiments impacting steel discs, yellow from impacting 3D printed plastic discs, and green markers from experiments using aluminium discs. Peak average pressures are found to deviate substantially from the previously found quadratic dependence on V for the centre and (to a lesser extent), the side pressures presented in figure 4(c).

4. Spatially integrated loading

4.1. Force measurements and impulse calculation

We perform force measurements on the discs to check to what extent they are consistent with the pressure measurements. Some typical force measurements are shown in figure 7(a). The main features of interest around the impact peak are the same as were found in pressure measurements. The first large peak results from the initial impact. Here however, the forces measured by the load cell are averaged throughout the disc & rod assembly that is mounted on the linear motor. As a result, structural vibrations in the impactor dominate the measured signals shortly after $t = 0$, and drown several weaker signals that might be of interest.

Force measurements were done using discs of different sizes and materials. The variation of peak forces with V is shown in figure 7(b). As with pressure measurements, force measurements at each set of parameters were repeated a number of times to obtain variance in the measurements. They are found to vary substantially from the quadratic scaling that peak pressures were found to follow. Instead, peak forces appear to grow as $\sim V^{1.54}$ within the experimental range of errors. Since experiments done with discs made of steel, aluminium, and plastic follow a consistent trend, we can conclude that the total force produced on the discs indeed have a hydrodynamic origin. They do not depend on the material that a disc is made from. The peak values' deviation from V^2 appear likely to be due to limited temporal resolution of the strain gauge load cell.

Notwithstanding the limited resolution of load cell, we can numerically integrate the force measurements starting from the time when the first impact peak starts to rise. The

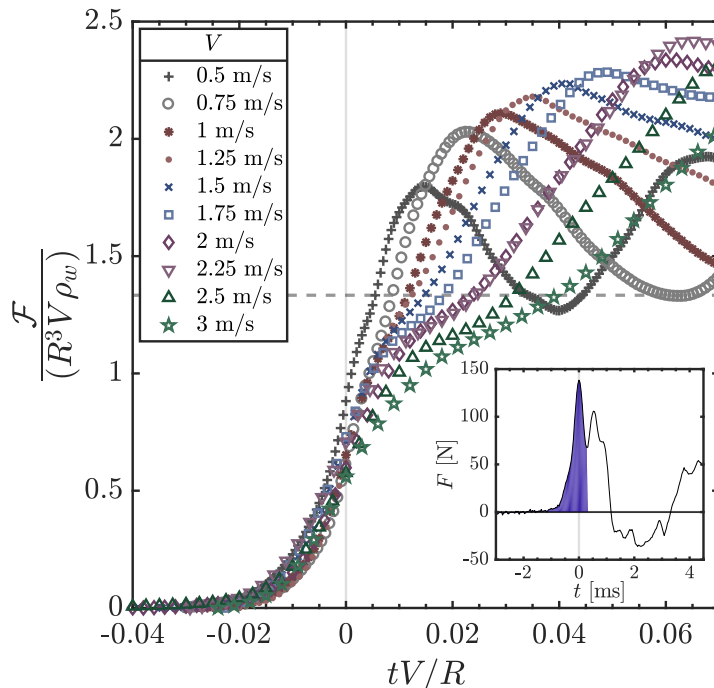


FIGURE 8. Non-dimensional force impulses $\mathcal{F}/R^3V\rho_w$ are computed from force measurements with a steel disc of radius $R = 4$ cm, impacting on water at various V . Each result is centred about $t = 0$ at the time of when the corresponding impact force attains its peak value. The horizontal dashed line is drawn to mark the non-dimensional force impulse value of $4/3$. Inset: A force-time curve at $V = 1$ m/s is shown; the shaded area shows the time-duration over which $F(t)$ is integrated to obtain \mathcal{F} .

force impulses

$$\mathcal{F}(t) = \int_{t_0}^t F(t') dt', \quad (4.1)$$

thus computed are non-dimensionalised as before using inertial length and time scales. The results are plotted in figure 8. As with pressure impulses, the growth of force impulses until the time of peak force (conveniently at $t = 0$) is well collapsed by the re-scaling. Our expectation from previous section (based on figure 6) is upheld by force impulse measurements.

After $t = 0$, the structural oscillations (signals with a period of 4 ms, visible both in figures 4(a-b) and 7(a)) become very large, and depending on its extent of submergence in the bath, are variedly affected by the bath's sloshing. Notice also in the inset of figure 8, that there is a secondary peak in the force, which cannot be easily ascribed to any hydrodynamic phenomenon. This explains why the later force signals and their resulting impulses do not follow hydrodynamic scales.

4.2. Impulse due to water impact of a disc

That at least in our experimental setup, both the pressure impulses $\Pi(t)$, and force impulses $\mathcal{F}(t)$ obey inertial scaling despite the presence of cushioning air layer, is an important observation as regards to comparing the measurements with theory. Here, we start with a brief discussion of the well-known idea of pressure impulse in a fluid. The idea is useful when fluid boundaries, or a portion of the bulk, is subjected to a sudden

acceleration of a large magnitude and short duration. Over this short duration, velocities of both the fluid and the boundary are small. Ignoring viscosity, Euler's equation, linearised in \mathbf{v} , can be used to describe fluid motion (Batchelor 1967; Cooker & Peregrine 1995)

$$\frac{\partial \mathbf{v}}{\partial t} = -\frac{1}{\rho_w} \vec{\nabla} p, \quad (4.2)$$

where both the terms are manifestly of large magnitude for a short interval of time, in which the acceleration term is dominant over the terms in Euler equation. Integrating both sides with time,

$$\mathbf{v}_{\text{after}} - \mathbf{v}_{\text{before}} = -\frac{1}{\rho_w} \vec{\nabla} \left(\int_{t_{\text{before}}}^{t_{\text{after}}} p(t') dt' \right), \quad (4.3)$$

which can be integrated and re-written in terms of a scalar flow potential ($\vec{v} = \vec{\nabla} \phi$) as

$$\phi_{\text{after}} - \phi_{\text{before}} = -\frac{1}{\rho_w} \left(\int_{t_{\text{before}}}^{t_{\text{after}}} p(t') dt' \right) \quad (4.4)$$

$$= \frac{\Pi(t_{\text{before}}) - \Pi(t_{\text{after}})}{\rho_w}. \quad (4.5)$$

This expresses that in a fluid that is initially stationary, any motion produced by sudden acceleration will, at least for a short duration, be irrotational. In such a fluid domain, flow potentials throughout the bulk are uniquely determined by the normal component of velocities imposed at its boundaries. In this context, the present experiment is especially well suited to testing pressure-impulse theory. The pressure impulse calculation that corresponds exactly to the present experiment with the impact of a disc shown in Batchelor (1967, section 6.10), yielding $\mathcal{F}_{\text{impact}} = 4/3 R^3 V \rho_w$. The same result was also arrived at in Lamb (1945, section 102) by deriving the kinetic energy that is imparted to the surrounding fluid by an immersed disc that is impulsively accelerated from rest. Glasheen & McMahon (1996) performed experiments impacting a disc on water, and measured the loss in its momentum from impact by measuring the sudden drop in its velocity (equation (4.3)). From the loss in the projectile's momentum, they estimated the added mass on the moving disc. The results were compared to the above analytical result (also in Birkhoff & Zarantonello (1957)), finding a good agreement.

Note that our method of computing the impact impulse differs significantly from that of Glasheen & McMahon (1996), who could calculate the force impulse by measuring the sharp drop in projectile momentum. Their method would not be suited in our case due to the amount of control in our experiment that allows us to impose a constant velocity. In contrast, we numerically integrate the directly measured force and local pressure over the duration of the impact peak. Moreover, our measurements extend the range of experimental parameters ($R^3 V \rho_w$) covered by Glasheen & McMahon (1996) to much larger disc momenta at impact.

We compute $\mathcal{F}_{\text{impact}}$ and Π_{impact} by considering the signal upto the end of the first peak (as shown in inset of figure 8). The latter are multiplied by the disc area to make the two measures of impact impulses comparable. The comparison is shown in figure 9. Note that the range of data for $\mathcal{F}_{\text{impact}}$ is greater than that for $\pi R^2 \Pi_{\text{impact}}$. This is due to the forces being measured with disc sizes up to $R = 8$ cm, while the pressures were measured with fixed disc size of $R = 4$ cm. It is seen in figure 9 that force impulses from our measurements lie very close to the theoretical prediction. We find good agreement between our data and the $4/3$ slope for small impact momentum ($\rho_w R^3 V$). However

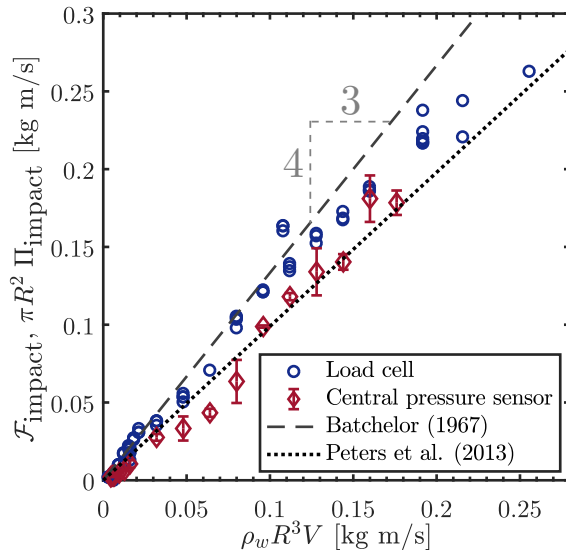


FIGURE 9. Impulses accumulated during the first impact peak (see inset of figure 8) are plotted against growth rate of the added mass of liquid at impact. Impulses calculated from pressure measurements (Π_{impact}) at the disc centre (shown in figure 6) were multiplied by the disc area so that they can be directly on the same scale as $\mathcal{F}_{\text{impact}}$. Dashed line shows the theoretical calculation for the impulse transferred from an impulsively accelerated disc to an infinite half-space filled with inviscid fluid. Dotted line is the result from *Peters et al.* (2013) (equation (4.6)).

at larger momenta, discrepancies set in, which cannot be solely attributed to limited temporal resolution of the sensors.

It is possible to at least approximately compute the influence of entrapped air layer on $\mathcal{F}_{\text{impact}}$, as was done by *Peters et al.* (2013), who calculated the total force on a disc with the cushioning air layer. They estimated the change in momentum of a disc slamming at constant velocity as

$$\mathcal{F}_{\text{impact}} = 0.315 \rho_w \pi R^3 V, \quad (4.6)$$

i.e., a reduction of the classical force impulse by about 25%. This result is also compared to our measurements in figure 9. It is found to lie closer to the area-integrated pressure impulses measured at the disc centre, but consistently below the directly obtained force-impulse data from the load cell.

5. Conclusions

We report here experiments where a flat disc is impacting at a controlled, constant velocity on a deep water bath initially at rest. We measure local pressures at the center and near to the edge of the disc, and the total impact force. At the moment of impact the disc entraps a thin air layer on the impacting side due to air-cushioning that occurs prior to the moment of first touchdown. The air layer causes a difference in impact pressures at the disc's centre and edge. We show that peak pressures due to impact at the disc centre scale as the square of the impact velocity. Peak impact pressures at the disc's edge are found to be a bit smaller, especially for higher impact velocities where the data depart from the V^2 scaling.

Pressure impulses $\Pi(t)$ are computed from measurements by numerically integrating them starting from the time they start to rise. The pressure impulse $\Pi(t)$ accumulated

at the disc centre are found to be higher than that at the disc edge. Further, the early growth stage of the central pressure impulse is found to be governed by inertial length and timescales. We are led to conclude that the initial loading at disc centre dominantly arises due to an inertial process, the added mass effect. The trapped air layer at impact, which is thickest at the disc's centre, mitigates pressure singularities and distributes the loading over the disc's surface. Its presence also prolongs the initial impact.

The impact pressures are compared with peak forces on the disc. The latter are found to not follow V^2 scaling, suggesting that they are severely under-resolved in time compared to the pressure measurements. Further, the role of added mass in producing the large initial impact force peak is verified by determining the force impulse $\mathcal{F}(t)$ at impact. As seen with $\Pi(t)$, the growth of $\mathcal{F}(t)$ is also well collapsed by a re-scaling with inertial length and time scales. Our analysis shows that impulses are a much more reliable, and reproducible indicator of the intensity of an impact event. This is especially the case when sensors are suspected to underestimate the peak pressures (or forces) due to their limited time resolution.

The impulses accumulated during the first peak, Π_{impact} and $\mathcal{F}_{\text{impact}}$, are compared to the theoretical hydrodynamic mass of the fluid that is accelerated by the impact. A better agreement is found between force impulses and the theory than by Glasheen & McMahon (1996), and over a much larger range of parameters. The Π_{impact} at disc centre are found to be consistently lower than both $\mathcal{F}_{\text{impact}}$ and the model. At disc momenta, the data increasingly deviate from the 4/3 slope, and follow a trend closer to the calculation by Peters *et al.* (2013).

Acknowledgements

We thank JM Gordillo for useful discussions. We acknowledge financial support from SLING (project number P14-10.1), which is partly financed by the Netherlands Organisation for Scientific Research (NWO). P.V-M acknowledges the support of the Spanish Ministry of Economy and Competitiveness through grants DPI2017-88201-C3-3-R and DPI2018-102829-REDT, partly funded with European funds.

Declaration of Interests

The authors report no conflict of interest.

REFERENCES

- ABRATE, S. 2013 Hull Slamming. *Applied Mechanics Reviews* **64** (6), 060803.
- BAGNOLD, R. A. 1939 Interim report on wave-pressure research. *Excerpt from the Journal of the Institution of Civil Engineers* .
- BATCHELOR, G. K. 1967 *An Introduction to Fluid Dynamics*. Cambridge University Press.
- BIRKHOFF, G. & ZARANTONELLO, E. H. 1957 *Jets, Wakes, and Cavities*. Academic Press.
- BOGAERT, H., LÉONARD, S., BROSSET, L. & KAMINSKI, M. L. 2010 Sloshing and scaling: results from the sloshel project. In *The Twentieth International Offshore and Polar Engineering Conference*. International Society of Offshore and Polar Engineers.
- BREDMOSE, H., BULLOCK, G.N. & HOGG, A. J. 2015 Violent breaking wave impacts. Part 3. Effects of scale and aeration. *Journal of Fluid Mechanics* **765**, 82–113.
- BREDMOSE, H., PEREGRINE, D. H. & BULLOCK, G. N. 2009 Violent breaking wave impacts. part 2: modelling the effect of air. *Journal of Fluid Mechanics* **641**, 389–430.
- BULLOCK, G. N., OBHRAI, C., PEREGRINE, D. H. & BREDMOSE, H. 2007 Violent breaking wave impacts. part 1: Results from large-scale regular wave tests on vertical and sloping walls. *Coastal Engineering* **54** (8), 602–617.

- CHAN, E. S., MELVILLE, W. K. & GASTER, M. 1988 Deep-water plunging wave pressures on a vertical plane wall. *Proceedings of the Royal Society of London. A. Mathematical and Physical Sciences* **417** (1852), 95–131.
- CHUANG, S. L. 1966 Experiments on Flat-Bottom Slamming. *Journal of Ship Research* **10** (1).
- COOKER, M. J. & PEREGRINE, D. H. 1995 Pressure-impulse theory for liquid impact problems. *Journal of Fluid Mechanics* **297**, 193–214.
- DENNY, D. F. 1951 Further experiments on wave pressures. *Journal of the Institution of Civil Engineers* **35** (4), 330–345.
- DIAS, F. & GHIDAGLIA, J. M. 2018 Slamming: Recent progress in the evaluation of impact pressures. *Annual Review of Fluid Mechanics* **50**, 243–273.
- ERMANYUK, E. V. & OHKUSU, M. 2005 Impact of a disk on shallow water. *Journal of Fluids and Structures* **20** (3), 345 – 357.
- FALTINSEN, O. M. 2000 Hydroelastic slamming. *Journal of Marine Science and Technology* **5** (2), 49–65.
- FALTINSEN, O. M., LANDRINI, M. & GRECO, M. 2004 Slamming in marine applications. *Journal of Engineering Mathematics* **48** (3-4), 187–217.
- GLASHEEN, J. W. & MCMAHON, T. A. 1996 Vertical water entry of disks at low Froude numbers. *Physics of Fluids* **8** (8), 2078–2083.
- HATTORI, M., ARAMI, A. & YUI, T. 1994 Wave impact pressure on vertical walls under breaking waves of various types. *Coastal Engineering* **22** (1-2), 79–114.
- HICKS, P. D., ERMANYUK, E. V., GAVRILOV, N. V. & PURVIS, R. 2012 Air trapping at impact of a rigid sphere onto a liquid. *Journal of Fluid Mechanics* **695**, 310–320.
- HULL, P. & MÜLLER, G. 2002 An investigation of breaker heights, shapes and pressures. *Ocean Engineering* **29** (1), 59–79.
- IAFRATI, A. & KOROBKIN, A. A. 2008 Hydrodynamic loads during early stage of flat plate impact onto water surface. *Physics of Fluids* **20** (8), 082104.
- JAIN, U. 2020 Slamming Liquid Impact and the Mediating Role of Air. PhD thesis, University of Twente.
- JAIN, U., GAUTHIER, A. & VAN DER MEER, D. 2020a Synthetic schlieren method using total-internal-reflection deflectometry, arXiv: 2009.00531.
- JAIN, U., NOVAKOVIC, V., BOGAERT, H. & VAN DER MEER, D. 2020b On wedge-slamming pressures, arXiv: 2011.10378.
- KAPSENBERG, G. K. 2011 Slamming of ships: where are we now? *Philosophical Transactions of the Royal Society A: Mathematical, Physical and Engineering Sciences* **369** (1947), 2892–2919.
- KIRKGÖZ, M. S. 1990 An experimental investigation of a vertical wall response to breaking wave impact. *Ocean Engineering* **17** (4), 379–391.
- LAMB, H. 1945 *Hydrodynamics*. Courier Corporation.
- MA, Z. H., CAUSON, D. M., QIAN, L., MINGHAM, C. G., MAI, T., GREAVES, D. & RABY, A. 2016 Pure and aerated water entry of a flat plate. *Physics of Fluids* **28** (1), 016104.
- MAYER, H. C. & KRECHETNIKOV, R. 2018 Flat plate impact on water. *Journal of Fluid Mechanics* **850**, 1066–1116.
- OKADA, S. & SUMI, Y. 2000 On the water impact and elastic response of a flat plate at small impact angles. *Journal of Marine Science and Technology* **5** (1), 31–39.
- PARTENSKY, H. W. 1989 Dynamic forces due to waves breaking at vertical coastal structures. In *Coastal Engineering 1988*, pp. 2504–2518. American Society of Civil Engineers.
- PEREGRINE, D. H. 2003 Water-Wave Impact on Walls. *Annual Review of Fluid Mechanics* **35** (1), 23–43.
- PEREGRINE, D. H. & THAIS, L. 1996 The effect of entrained air in violent water wave impacts. *J. Fluid Mech.* **325**, 377–397.
- PETERS, I. R., VAN DER MEER, D. & GORDILLO, J. M. 2013 Splash wave and crown breakup after disc impact on a liquid surface. *Journal of Fluid Mechanics* **724**, 553–580.
- RICHERT, G. 1969 Experimental Investigation of Shock Pressures Against Breakwaters. In *Coastal Engineering 1968*, pp. 954–973. American Society of Civil Engineers.
- SMITH, N. J., STANSBY, P. K. & WRIGHT, J. R. 1998 The slam force on a flat plate in free flight due to impact on a wave crest. *Journal of Fluids and Structures* **12** (2), 183–196.
- TÖDTER, S., EL MOCTAR, O., NEUGEBAUER, J. & SCHELLIN, T. E. 2020 Experimentally

- Measured Hydroelastic Effects on Impact-Induced Loads During Flat Water Entry and Related Uncertainties. *Journal of Offshore Mechanics and Arctic Engineering* **142** (1).
- VERHAGEN, J. H. G. 1967 The Impact of a Flat Plate on a Water Surface. *Journal of Ship Research* **11** (4).
- WOOD, D. J., PEREGRINE, D. H. & BRUCE, T. 2000 Wave Impact on a Wall Using Pressure-Impulse Theory. I: Trapped Air. *Journal of Waterway, Port, Coastal, and Ocean Engineering* **126** (4), 182–190.